CORTEX 95 (2017) 238–247

Available online at www.sciencedirect.com

ScienceDirect

Journal homepage: www.elsevier.com/locate/cortex

Clinical neuroanatomy

Whole network, temporal and parietal lobe contributions to the earliest phases of language production

Alessandro Principe [a,*], *Marco Calabria* [b], *Adrià Tauste Campo* [b,c], *Josephine Cruzat* [b], *Gerardo Conesa* [d], *Albert Costa* [b,e] *and Rodrigo Rocamora* [a]

[a] *Epilepsy Unit, Neurology Dept., Hospital Del Mar, Parc de Salut Mar, Barcelona, Spain*
[b] *Center for Brain and Cognition, Pompeu Fabra University, Barcelona, Spain*
[c] *IMIM, Parc de Salut Mar, Barcelona, Spain*
[d] *Neurosurgery Unit, Hospital Del Mar, Parc de Salut Mar, Barcelona, Spain*
[e] *Institució Catalana de La Recerca I Estudis Avançats (ICREA), Barcelona, Spain*

ARTICLE INFO

Article history:
Received 24 December 2016
Reviewed 8 March 2017
Revised 6 May 2017
Accepted 15 August 2017
Action editor Marco Catani
Published online 24 August 2017

Keywords:
Picture naming
Language
SEEG
Error prediction
Brain networks
Anatomical hubs

ABSTRACT

We investigated whether it is possible to study the network dynamics and the anatomical regions involved in the earliest moments of picture naming by using invasive electroencephalogram (EEG) traces to predict naming errors. Four right-handed participants with focal epilepsy explored with extensive stereotactic implant montages that recorded temporal, parietal and occipital regions -in two patients of both hemispheres-named a total of 228 black and white pictures in three different sessions recorded in different days.

The subjects made errors that involved anomia and semantic dysphasia, which related to word frequency and not to visual complexity. Using different modalities of spectrum analysis and classification with a support vector machine (SVM) we could predict errors with rates that ranged from slightly above chance level to 100%, even in the preconscious phase, i.e., 100 msec after stimulus presentation. The highest rates were obtained using the gamma bands of all contact spectra without averaging, which implies a fine modulation of the neuronal activity at a network level. Despite no subset of nodes could match the whole set, rates close to the best prediction scores were obtained through the spectra of the temporal-parietal and temporal-occipital junction along with the temporal pole and hippocampus. When both hemispheres were explored nodes from the left side dominated in the best subsets. We argue that posterior temporal regions, especially of the dominant side, are involved very early, even in the preconscious phase (100 msec), in language production.

* *Corresponding author*. Epilepsy Unit, Neurology Department, Hospital Del Mar, Parc de Salut Mar, Barcelona, Spain.
E-mail address: aprincipe@parcdesalutmar.cat (A. Principe).

http://dx.doi.org/10.1016/j.cortex.2017.08.021
0010-9452/

1. Introduction

Information about how the speech production system works comes from many different sources—from the study of aphasic patients to brain imaging techniques (e.g., DeLeon et al., 2007; Dell, 1990; Fromkin, 1971; Garrett, 1980; Graves, Grabowski, Mehta, & Gordon, 2007; Hickok & Poeppel, 2007; Munding, Dubarry, & Alario, 2016; Wilson, Isenberg, & Hickok, 2009). This information has helped to delineate the spatiotemporal brain dynamics of how people produce language. (e.g., Blackford, Holcomb, Grainger, & Kuperberg, 2012; Costa, Strijkers, Martin, & Thierry, 2009; Laganaro and Perret, 2011; Strijkers & Costa, 2016). However, we are still far from having a complete understanding of the brain dynamics behind this unique human ability.

Here we explore the brain dynamics during speech production using invasive EEG (iEEG). Despite the advantages that this technique offers in terms of temporal and spatial resolution, few studies have made use of it to explore the brain dynamics involved in speech production (e.g., Cho-Hisamoto, Kojima, Brown, Matsuzaki, & Asano, 2015; Edwards et al., 2010; Hamamé, Alario, Llorens, Liégeois-Chauvel, & Trébuchon-Da Fonseca, 2014; Llorens, Trébuchon, Liégeois-Chauvel, & Alario, 2011; Martin, Millán, Knight, & Pasley, 2016; Tanji, Suzuki, Delorme, Shamoto, Nakasato, 2005). In particular, we study the neuroanatomical involvement of parietal, occipital and temporal structures during speech production by means of a picture naming task. We assess the iEEG of four patients implanted because of their intractable epilepsy. We focus on the brain indexes associated with failures to correctly name the pictures. That is, we compare the brain activity elicited by correct versus incorrect naming instances as a proxy for speech production processes. Hence, we assess when and where iEEG activity allows classifying correct versus incorrect responses, an approach so far not described in literature.

It is important to mention that instead of using grid electrodes, we explore patients with stereotactically implanted electrodes, which allows displaying the electrophysiological activity in a volumetric fashion. Moreover, Instead of relying on averaging repetitions like in ERPs studies, we decided to tap the differences between stereotactic-EEG (SEEG) traces before and after the stimulus presentation for predicting an event like in a brain-computer-interface approach.

To advance our results, we are able to distinguish between correct versus incorrect naming instances just a few milliseconds after the picture presentation and more than half a second before the actual patients' responses. This classification was achieved by assessing the activity of the gamma and beta bands. Furthermore, we were able to track which anatomical hubs are more sensitive to this classification—different sections of the temporal lobe at different times.

2. Patients and methods

This study was approved by The Clinical Research Ethical Committee of the Municipal Institute of Health Care (CEIC-IMAS). Patients were informed about the procedure and gave written consent before the experiment. For this study we selected four right-handed subjects with drug-resistant focal epilepsy who presented automotor seizures and an alteration of the language domain at the neuropsychological examination that spanned from none to moderate. All patients were Spaniards and fluent in Spanish. Two of them presented a right temporal lobe epilepsy (R1 and R2), the other two a left temporal lobe epilepsy (L1 and L2). In two cases, L2 and R1, there was an involvement of the mesial structures, while in the other two the seizure onset zone was located in the temporal posterior and basal regions (see Table 1 for more information). Patients were selected because of the extensive electrode coverage of the parietal, temporal and occipital regions. Two of the four subjects (L1 and R1) were explored in both hemispheres (see Fig. S1 of Section 9 for more information about the electrode position).

All recordings were performed using a standard clinical EEG system (XLTEK, subsidiary of Natus Medical) with a 500 Hz sampling rate. A uni- or bilateral implantation was performed using 12–16 intracerebral electrodes (Dixi Médical, Besançon, France; diameter: .8 mm; 5–15 contacts, 2 mm long, 1.5 mm apart) that were stereotactically inserted (thence the name stereotactic-EEG or SEEG) using robotic guidance (ROSA, Medtech Surgical, Inc). In all patients we recorded 126 channels (maximal amplifier allowance) and discarded the less informative contacts by visual inspection before the recording start. The decision to implant, the selection of the electrode targets and the implantation duration were entirely made on clinical grounds without reference to this research study.

Only patient R1 was recently intervened and has been seizure free for 4 months (Engel 1A). Patient L2 is currently seizure free 16 months after thermocoagulation. Patients L1 and R2 are awaiting surgery.

2.1. *Picture naming task*

In the picture-naming task participants were asked to name 228 pictures presented in three different blocks in two different days. Pictures were black and white line drawings of familiar objects from a wide range of semantic categories

Table 1 – Patients are divided in two groups, L1 and L2 with left temporal lobe epilepsy, R1 and R2 with right temporal lobe epilepsy.

Subject	Sex	Handedness	Electrodes (right)	Epilepsy onset zone	Reaction time (average ± SD ms)	Accuracy %	Anomia %	Semantic %
L1	Female	R	11 (4)	Left hippocampus and temporal cortex	952 ± 149	69	72	28
L2	Male	R	13	Left temporal cortex	888 ± 234	61	83	17
R1	Male	R	3 (9)	Right hippocampus	880 ± 140	93	83	17
R2	Male	R	0 (15)	Right temporal basal cortex	850 ± 113	94	50	50

selected from the Snodgrass and Vanderwart (1980) set. Each picture appeared once centrally and sequentially on the computer screen in a pseudo-random order for 2000 msec followed by a fixation cross for 1000 msec. Participants were instructed to overtly name every item as fast and accurately as possible in Spanish. The task was presented using a script written in Processing 2.2.1 running on a laptop computer (MacBook Pro, Apple inc., CPU: Intel i7 series) located approximately 60 cm away from the patient. The script was responsible to orchestrate the picture presentation and a feedback to the EEG amplifier in the form of a transistor transistor logic (TTL) signal produced by a Genuino UNO (Arduino LLC, open-source hardware distributed under Creative Commons) microcontroller and reduced to 5 mV by hardware resistors. The accuracy was scored manually by the experimenter and later reviewed by two neuropsychologists (MC and JC).

2.2. EEG processing, error classification and anatomical hubs

Two epileptologists (AP and RR) reviewed the EEG traces using the Natus software to classify interictal activity. No relation was found between spike and spike-wave discharges and the trial outcome, therefore we did not exclude any trial from analysis.

2.2.1. EEG processing

We summarise the EEG processing in Fig. 1. To remove the alternate current contamination the continuous SEEG data was notch filtered at 50, 100, 150 and 250 Hz. No special montage was used and all analyses were performed using the original extracerebral referenced traces, bandpass filtered at .5–250 Hz using a butterworth filter. In order to have specific

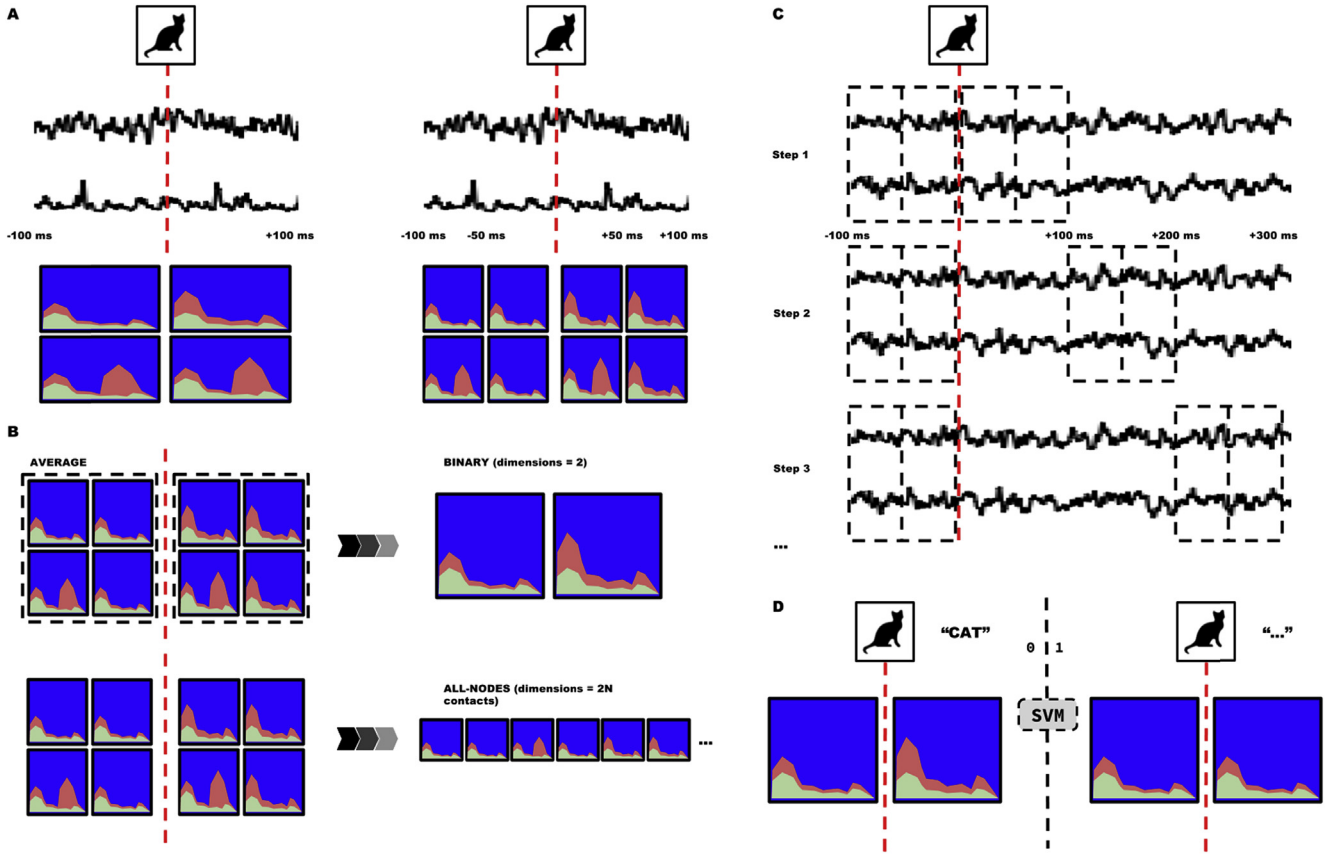

Fig. 1 – EEG processing and error classification. A. To reduce spectra alteration from spikes we splitted 100 msec windows before and after stimulus presentation, here presented as the silhouette of a cat. To simplify, in the graphic we show only 2 EEG channels, the bottom presenting interictal activity. On the left we show the spectra relative to 100 msec windows, while on the right we present the spectra relative to splitted windows. Using the 100 msec we would average 4 spectra, 50% of them altered by a spike, while using the 50 msec windows we would average 8 spectra, only 25% of them altered by interictal activity. B. To produce the vectors used for training the classifier and predict errors we used two strategies: in the *binary* we averaged all pre-stimulus trials and all post-stimulus trials into a bidimensional vector; in the *all-nodes*, on the other hand, we produced vectors using 252 dimensions, which is twice the number of contacts, since we use all spectra from the pre-stimulus and the post-stimulus epochs. C. Window steps: at all steps we compared the same basal pre-stimulus window versus a 100 msec post-stimulus window that we slided at each step by 100 msec up to 700 msec. As explained in panel A, to obtain spectra we used 50 msec windows, thus we graphically represented the window as splitted rectangles. D. Support vector machine (SVM) analysis: we trained the classifier using correct and error naming trials as two different classes. In the figure we show an example of anomia using the *binary* vectors.

spectral information we calculated the spectra of all channels and trials using a sliding, non-overlapping window of 50 msec. We used the *Welch* method (Welch, 1967) to compute the estimate of the power spectral density. We chose this window size in order to minimise interictal activity spectral distortion as shown in Fig. 1A, where we plot a simplified EEG constituted by two channels, one of them presenting spikes. By definition spikes are rapid burst of high frequency activity that last less than 70 msec. Actually, the majority of spikes last less than 50 msec. In the example, a 100 msec window would be altered by interictal activity, instead by using 50 msec we would obtain spectra of normal activity aside of altered spectra. In the figure we show how it is more likely to average spectra altered by interictal activity by using 100 msec windows. Technically, the interictal activity minimisation takes place in the second step, illustrated in Fig. 1B.

2.2.2. *Error classification*

Machine learning classifiers use vectors (lists of numbers that represents features) to compute the differences between classes. To reduce the spectra of all channels to numerical vectors we considered two different approaches. In the *binary* approach we averaged all pre-stimulus and all post-stimulus spectra of all channels. By averaging we could reduce the weight of altered spectra (less represented than the unaltered ones) and also reduce the set to a bidimensional vector (the simplest possible for classification purposes). In the *all-nodes* approach we created vectors containing the series of all spectra. This approach considers a high dimensionality feature vector (equal to twice the number of contacts, since we use all spectra from the pre-stimulus and the post-stimulus epochs) of which less represented features (in this case the altered spectra) will be given less statistical power by the classifier. In Fig. 1C, we show how we computed the window steps. We considered the following time steps from stimulus presentation: 100, 200, 300, 400, 500, 600 and 700 msec. We selected these steps after processing the behavioural statistics that showed an average response rate higher than 800 msec. At each step we considered two pre-stimulus windows against two post-stimulus windows, e.g., at step 100 we included the following windows: −100 to −50, −50 to 0, 0 to 50 and 50 to 100 msec. For the error prediction we used a *support vector machine* (SVM; Schölkopf & Smola, 2002) implemented in a hybrid C/Python library frequently used in machine learning problems (Scikit-learn; Pedregosa et al., 2011). SVMs are especially useful when the supervised classification involves binary choices and/or trees (Cortes & Vapnik, 1995). To create the models the classifier was trained with correct (the patient correctly names the picture) and naming error trials as two different classes, as shown in Fig. 1D. We used either the *binary* or the *all-nodes* vectors in distinct experiments. As a final step before training the SVM, of each spectrum in either *binary* or *all-nodes* vector we chose a band, either beta (15–30 Hz), gamma (30–80 Hz) or ultra-gamma (80–120 Hz) and averaged their values. Data from patients was analysed separately and then grouped. Only in one experiment we built a set containing the data of all trials recorded from all contacts from the four patients, the *all-patients-all-trials-all-nodes* set. For building the models we used either a *linear* or *radial basis function* kernel. Both gave similar results in this setting, therefore we only present values obtained with the latter.

2.2.3. *Anatomical hubs*

To determine anatomical hubs we used Monte Carlo testing. We took 1000 random subsets of 10% of contacts (nodes) of each patient and run analyses with *all-nodes* vectors at 100 and 500 msec using the gamma band. No repetition of nodes was allowed, therefore we calculated that each node would be represented in the random subsets an average of 10 times and the chance of analysing the same subset would be infinitesimal ($\sim 1.05 \cdot 10^{-27}$). After acquiring the results we redistributed the accuracy rates between nodes, i.e., we assigned to each node the accuracies obtained in every explored subset in which the node was present, and sorted the nodes from best to worst average accuracy rates. To divide *accuracy groups* we took each sorted distribution and progressively divided them from the top by comparing equally sized subgroups starting from 3 items. A group was defined when the null-hypothesis chance (p value) increased after reaching the smallest value during the size increase, then the best subgroup was excluded and the analysis repeated on the remaining nodes until the worst subgroup size fell below 3, i.e., when all nodes were considered and no further divisions were possible.

2.2.4. *Spectra reconstruction*

After assessing the error prediction accuracies and most informative anatomical hubs we calculated trial spectra. We first divided all trials between correct and error trials, then we averaged the best channels (from *accuracy groups*) of temporal pole, second temporal gyrus, temporal basal, hippocampus head and tail, temporal junction, lateral parietal and occipital lobe. In this way, for each region we produced two spectra per patient representing the 200 msec before and the 200 msec after stimulus presentation. In this way we translated accuracy rates as band power activations.

2.3. *Image reconstruction and modelling*

To identify the anatomical position of the electrode contacts we used the 3D Slicer software (Pieper, Halle, & Kikinis, 2004). With the registration tool we coregistered (rigid body, 6° of freedom) the post-implantation computerised tomography (CT) scan to the pre-implantation magnetic resonance imaging (MRI). We then added the electrode fiducials on a glass model of each patient's brain obtained with the segmentation tool of the Freesurfer bundle (Fischl, 2012). To obtain a single model we coregistered all studies on the MNI152 template provided by the Freesurfer bundle using a semi-automated registration process of 3D Slicer. Briefly, we calculated a linear transform with 12° of freedom by superposing and morphing each patient's brain MRI onto the MNI brain template, then we used the transform matrix to translate, shift, skew and resize all other studies (CT scan, and unaltered MRI) accordingly. Since the 3D Slicer interface shows the MNI coordinates when hovering the mouse pointer, we could identify structures touched by electrode contacts both by visual inspection and by referring to the aforementioned coordinates. See Section 9 for information about a double check with the SPM tool (Eickhoff et al., 2005).

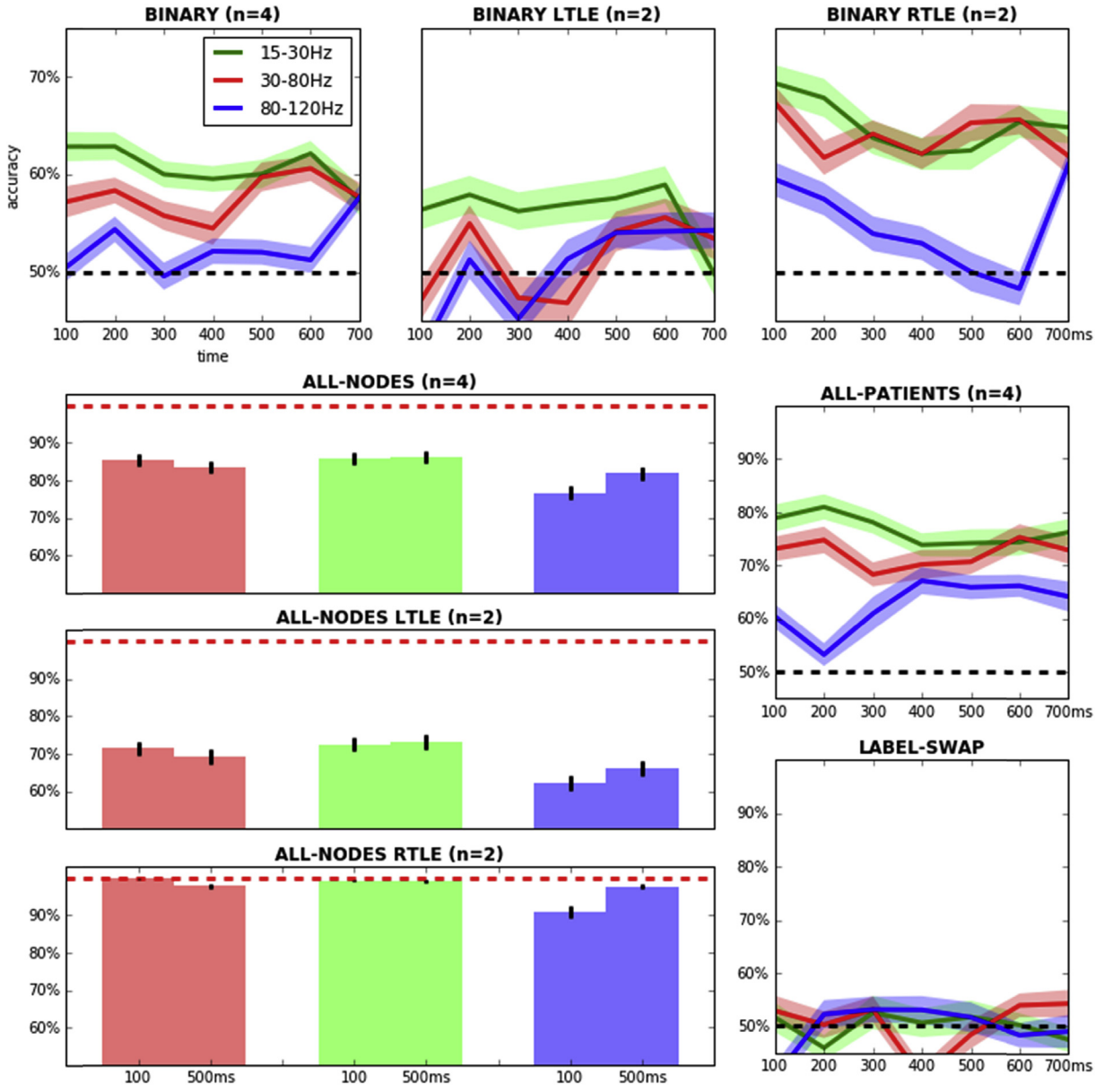

Fig. 2 – Prediction rates using the different methods. The *binary average* uses only two values per trial, while the *all-nodes* uses a vector containing the values of all channels and windows (see Section 2.2 for more details). We present separately overall, LTLE and RTLE results for each method. The *all-patient* plot represent accuracy rates at all times by mixing all trials and nodes from the four patients as if they were a single subject (*all-patients-all-trials-all-nodes* set in the text). To check for possible learning biases we applied the label swapping method to the latter (label-swap plot). Black dotted lines represent chance level, while red dotted lines represent full prediction rates (100%). Error bars and line halos represent SEMs. In *binary* and *all-nodes* experiments, they represent the differences between subjects; in *all-patient* and *label-swap* they represent the deviations of 1000 replicas.

2.4. *Statistical analyses, bootstrapping and anatomical hubs*

To understand whether the naming errors were related to either visual complexity or word frequency we separated all trials of all subjects into two groups (correct and error trials) and checked whether there were significant differences in the distribution of the two aforementioned variables.

For the error prediction models we balanced the sets using a hybrid all-samples/bootstrapping technique. To ensure that all error and correct trials were considered in every analysis we first shuffled the error set (always the smaller in size) and then added error trials from the original set by random sampling with replacement (Efron, 1992) until the number of error trials reached the number of correct trials. The balancing allowed a better training and shortcutted the need to calculate

receiver operating characteristic area under the curve (ROC AUC) rates since they would match the accuracy rates. To ascertain any bootstrap procedures bias we conducted several tests with label permutation. By swapping the category labels, this procedure detects learning procedure effects. When the latter are present prediction rates fail to drop to chance level.

To cross-validate our results we used the k-fold method (Dong & Han, 2004). Briefly this technique divides the data into k different subsets and creates k models with k−1 subsets to be tested against the remaining subset. For our analyses we used $k = 10$.

Mann Whitney *U* and *t*-test were performed accordingly to distributions. To check for Gaussian distribution we used the Shapiro–Wilk normality test.

3. Results

3.1. Naming errors were related to word frequency

The error rate across the four subjects was 21%, unevenly distributed between left and right temporal lobe epilepsy (35% *vs* 7%). Errors were of different type but anomia was the most prevalent type by far (see Table 1 for more information).

At least two loci may be identified as the origin of the errors while naming a picture: from visual processing or from more language-dependent sources. We looked at the effect of visual complexity as a proxy of visual demand in naming, but we did not find any differences in the distribution of this parameter between errors and correct responses. However, when we used word frequency, as a variable more related to language processing, we found that errors were more associated to low frequency words than correct responses (22.3 ± 1.13 *vs* 15.9 ± 1.82 average word frequency ± SEM, $p = .0003$).

3.2. The modulation of gamma and beta bands at a network level allows error prediction

In this phase we used both the *binary* and the *all-nodes* vectors. Both analyses considered all channels of the SEEG but with different strategies. The *binary* trained the classifier with averaged bidimensional vectors, of which one dimension corresponded to the 100 msec previous to the stimulus and 100 msec in the post-stimulus epoch respectively, while the *all-nodes* trained the classifier to recognise a multidimensional feature space containing all pre-stimulus and all post-stimulus spectra.

The first interesting result concerns the marked differences between left and right temporal lobe epilepsy (L and RTLE) patients. In LTLE the prediction was far worse and did not significantly overcome chance level (50% for a binary distribution). Although not totally unexpected, it is remarkable that the worse rates in LTLE were found to be the earliest ones using the *binary* vectors. All considered bands showed two peaks of processing activity, one in the earliest 100 msec (200 msec for LTLE subjects) and the second around 400–600 msec. Therefore we furthered our analysis by using the *all-nodes* approach at 100 and 500 msec. Training the classifier with data from all contacts dramatically increased the classification power, which reached 100% in RTLE patients, at 100 msec in the gamma band (Fig. 2), while LTLE patients error prediction rates rose above 70%, at least in the gamma and beta bands. Interestingly, in these patients the beta band was more informative than the gamma band. The latter though retained a certain specificity for the 100 msec step.

Finally, to understand whether this effect could be generalised across patients, we made an *all-patients-all-trials-all-nodes* set that we analysed at beta, gamma and ultra-gamma bands. In other words, we collected all trials from all patients and analysed them as if they were recorded from a single subject. Surprisingly, the rates dropped only to around 75% and again the peaks were distinguishable at 100 and 400–600 msec. To check whether these results were not depending on the method, especially the bootstrapping procedure, we analysed the *all-patients-all-trials-all-nodes* set using label swapping, which made rates drop to chance level. We repeated this procedure 1000 times and no permutation overcame benchmark rates at any time step ($p < .001$).

3.3. Whole network effect and anatomical hubs

In this context we use error prediction as a synonym of labelling accuracy. Formally the algorithm is trained to recognise patterns that precede a naming error, therefore a correct labelling corresponds to a prediction. No subset of contacts could produce error prediction rates matching the rates obtained through the original set using the *all-nodes* analysis. Despite that, certain combinations allowed accuracies that almost reached the best results. In other words, accuracy groups list contacts in order of error prediction power. To summarise this contribution we depicted all nodes taking part in the first *accuracy group* of each patient into a glass model that shows snapshots of the brain activity at 100 and 500 msec after stimulus presentation (see Fig. 3, circles represent the activation at 100 msec, squares at 500 msec). Interestingly, in the early phase of naming both posterior (occipital and parietal), junctional (angular gyrus and temporal-occipital junction) and anterior structures (temporal pole, temporal basal and hippocampi) together present the best prediction power. Several hundreds of milliseconds after (at 500 msec) the fulcrum shifts towards anterior structures, especially the temporal and temporal basal gyra, although prediction power of the junctional structures remains maximal. When both hemispheres were explored, structures of the dominant side were more likely among the most important prediction hubs. When only the right hemisphere was explored (subject R2) the number of nodes distributed among the first two *accuracy groups* was increased (16.0 ± 10.0 *vs* 5.5 ± 4.4 contacts, median ± SD, $p < .05$).

3.4. Complex beta and gamma modulation

To understand which kind of modulation allowed us to predict the trial outcome with good confidence rates, we tracked the anatomical structures most likely responsible for the prediction at 100 and 500 msec by ordering the most informative contacts. Structures from the right or left hemisphere could be selected depending on the electrode coverage and prediction scores in the accuracy groups. Fig. 4 shows spectra before and after stimuli, each line represent a subject, the first column displays the averages of all correct trials, while the second the

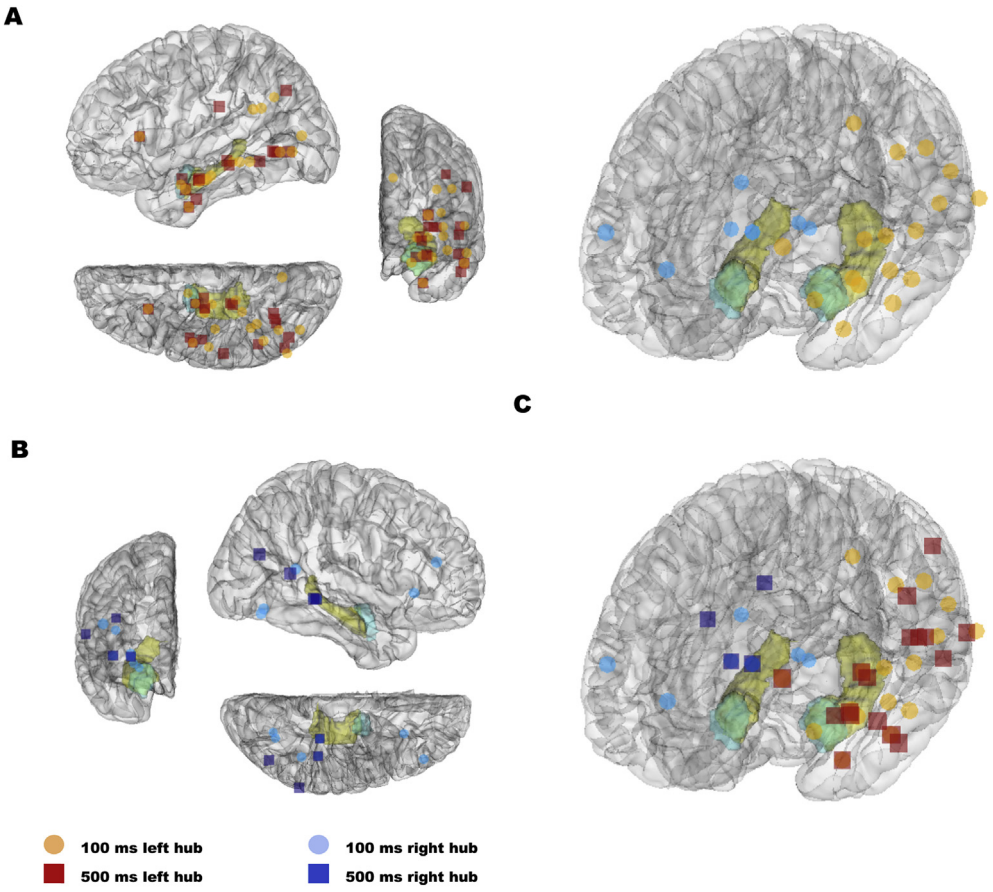

Fig. 3 – Brain regions by prediction accuracy, some nodes (hubs) presented higher accuracy rates than the rest (see Section 2.2 for more information). Panel A shows the left hemisphere contribution to error prediction, while panel B the right hemisphere contribution. Panel C shows two snapshots of the whole glass model, top yawed and down-pitched towards the left. The top model only depicts the 100 msec accuracy groups, while the bottom model represents both 100 and 500 msec accuracy groups.

averages of all wrong trials. For subjects L1 and L2 only left sided structures were chosen because only left sided structures listed in the first accuracy group. For subject R2, the temporal areas of the dominant side were selected. In this patient the junctional and posterior areas were mapped only on the right hemisphere. All subjects showed a gamma and/or beta band modulation of anterior temporal, hippocampal tail and parietal-occipital regions before naming correctly a picture. RTLE patients, especially R2, showed the highest amount of positive modulation in the temporal junction and parietal regions. The modulation somehow reverses before an error, especially in LTLE patients. RTLE subjects still show a positive modulation that somehow mimics the one that occurs in correct trials, but to a lesser extent. Since RTLE implants did not (R2) or only partially covered the left temporal junction and parietal lobe, the spectra of these subjects show the activation of posterior right structures. These results suggest that posterior structures from the dominant or non-dominant hemisphere participate differently in picture naming.

4. Discussion

In the study we investigated whether it is possible to assess the network dynamics and the anatomical regions involved in the earliest moments of picture naming by using SEEG. The results suggest that brain activation in occipital, parietal and temporal areas can be used to predict the success of word retrieval.

As expected, beta and gamma activity increased in these brain areas when subjects successfully named a picture as compared to when they made an error. Furthermore, this prediction can already be made recording the activation a few milliseconds after the naming process has started and much earlier than the response is given – just as soon as 100 msec after the picture is shown. These observations were obtained by analysing the spectra of SEEG traces before and after the picture presentation for trials than led to correct and incorrect responses. We trained a classifier to tease apart both sets of trials using a portion of the bands averaged from the spectra. We assessed the classifier accuracy by looking at how well it classifies trials that were not used for the training.

The fact that the prediction can be made by looking at the state of the network very early on suggests that conscious access to the picture semantic representation has not been yet achieved. This interpretation is based on studies using iEEG and MEG that have shown that the neurophysiological correlates of conscious perception of very simple visual cues differ from the unconscious perception at least 100 msec after the stimulus presentation and are followed by an increase of theta

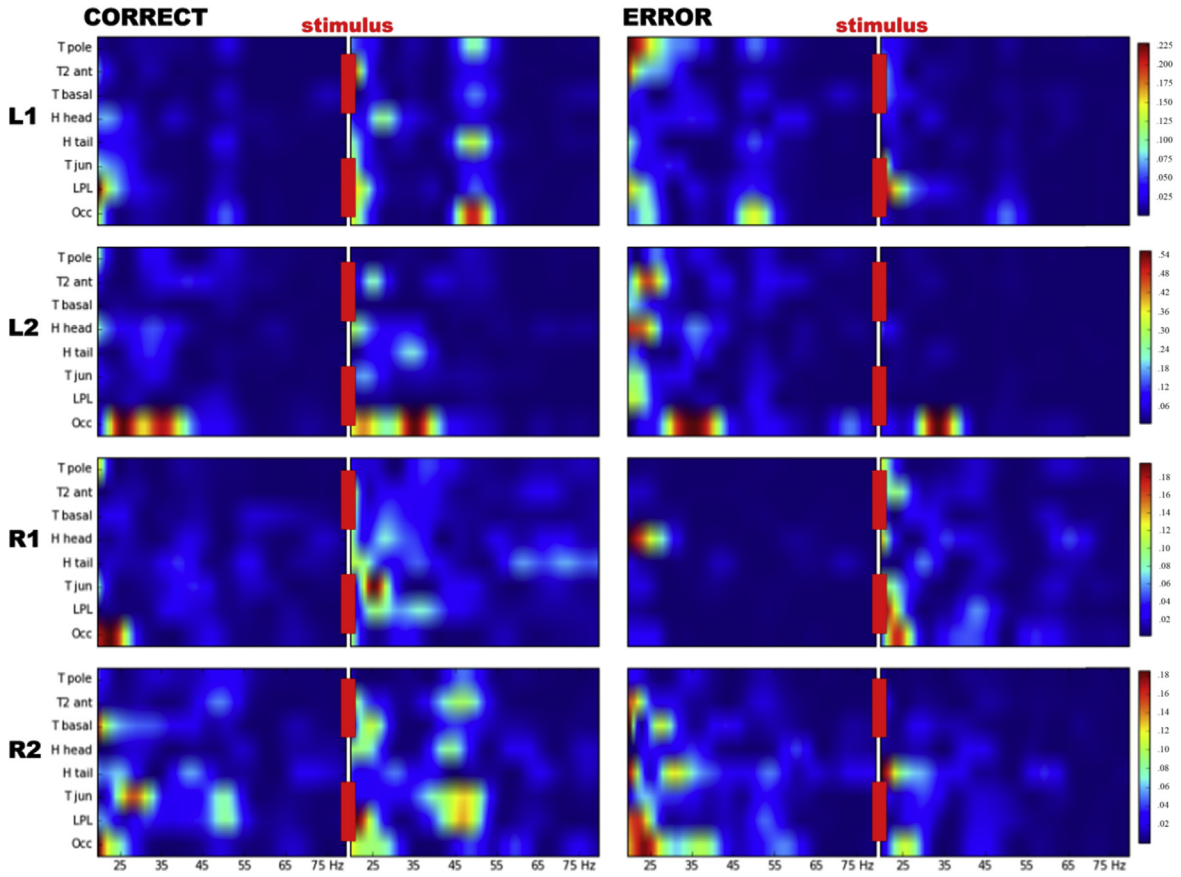

Fig. 4 – Spectrograms of selected brain regions: temporal pole (T pole), anterior temporal gyrus 2 (T2 ant), temporal basal (T basal), hippocampus head and tail (H head and tail), lateral parietal and occipital lobe (LPL and Occ). Columns depict changes in beta and gamma bands after stimulus presentation. The first column represent the averages of correct trials, while the second column the averages of error trials. Colours of the scale represent power spectra density (PSD [V2/Hz]) ranges.**

activity in the ventral striatum at 200 msec (Salti et al., 2015; Slagter et al., 2017). Therefore more complex visual stimuli should be consciously perceived at least at the same latency, if not later.

We also observe that the highest predictive power of the classifier is found when using the entire set of contacts. This supports the notion that picture naming is sustained by a distributed brain network that is rapidly activated in the course of language production (Chao, Haxby, & Martin, 1999; Wilson et al., 2009). Notwithstanding the existence of this distributed network, we also observed some major hubs participating in the naming process. Indeed, when the classifier was trained with certain contact combinations performed almost as well as the classifier trained with the whole set. This reveals that there are hubs processing the most important information for distinguishing between correct and incorrect responses.

One of the most interesting results was that using random distributions we could demonstrate a spatial shift of prediction power, from more posterior towards anterior regions of the temporal lobe, through time. The late (500 msec) distributions involved predominantly the pole, lateral and basal areas of the dominant temporal lobe, as expected (Chao et al., 1999). As we know, language production is sustained by a large distributed brain network, but the exact time-course is not completely known (for a review see Indefrey & Levelt, 2004). Here, we tried to couple these two information and we found that different brain areas are involved in time-course from 100 to 500 msec, and their activation is predictive of the subjects' response. This is relevant within the literature of SEEG and language because it adds new evidence of the early processing of language, beyond what we already know from previous studies (e.g., Edwards et al., 2010; for a review see Llorens et al., 2011).

Two more interesting findings are related to the differential contribution of hemispheres during picture naming and the consistency in the predictive power of the classifier.

Indeed, the number of contacts needed to distinguish errors from correct naming instances was higher for the right hemisphere as compared to the left one. This reveals that more nodes of the non-dominant hemisphere are needed to achieve the same results in error prediction.

About the consistency across time and across subjects, the predictability of errors did not decrease when we considered all trials (performed in different days) and all patients together (*all-patients-all-trials-all-node* vectors). This reveals a clearcut difference between the activation of cortical areas when naming is successful versus a failure of the process to retrieve the information. This suggests that brain dynamics behind the processing of naming can be compared between subjects

using machine learning methods, despite the differences in electrode placement, their physiological and pathophysiological background.

However, there is also an important caveat to mention. The source of the differences between correct and incorrect trials comes mostly from anomias for low frequent words, a condition known to be more demanding for lexical retrieval because of the involvement of control processes (for error-related brain areas and cognitive processes see Corina et al., 2010). Since we were not able to measure the contribution of such non-linguistic components with a control task, we need to acknowledge that our findings cannot be interpreted exclusively in terms of linguistic processes.

The approach of analysis used in our study was to investigate how early network dynamics can predict the success of word retrieval. Therefore, as first attempt we concentrated the analysis on more frequent errors we found in our patients, that is anomias (from 50% to 83%), and not considering semantic paraphasias because they were only 20% in most of the patients. Further research will focus on prediction of network dynamics by comparing different types of errors in order to disentangle the contribution of other linguistic components, such as semantics, phonology and motor planning of speech.

Another important aspect to investigate further concerns the differences between RTLE and LTLE patients. Despite error rates in LTLE were expected, further studies with more subjects and more trials should determine whether the error prediction differences between RTLE and LTLE subjects relate to the increased error rates of the LTLE group, or represent the hallmark of physiopathological mechanisms. Moreover, future studies are needed to determine whether this kind of analyses might help defining eloquent areas, which is of paramount importance for epilepsy surgery. Unfortunately we cannot answer this question with this small set of LTLE subjects, who in addition have not been operated for different reasons.

From the technical point of view, our study also contributes to the general research of iEEG, by showing the usefulness of analysing SEEG traces without electrical stimulation in the context of language processing. This has allowed us to define in a more fine-grained manner the time course, since previous studies using iEEG did not usually consider activations before 150 msec after stimuli (Cho-Hisamoto et al., 2015; Tanji et al., 2005). To show the usefulness of SEEG trace analysis is important because this technique provides a very large number of recording points distributed in a more volumetric way, which therefore can be used to better describe the cortical networks involved in cognitive processes.

5. Conclusions

This study shows how SEEG analysis and machine learning methods can be combined in a successful way to understand the dynamics of brain networks behind cognitive processes. This combination allowed us to highlight a complex modulation of the brain electrical activity that takes place preferentially in temporal and parietal structures of the dominant side. This processing occurs very early in picture naming, in a pre-conscious phase, and consolidates in a second peak, possibly related to conscious perception. Further studies using this kind of error analysis might pave the way for the development of tools useful in the clinical setting.

Funding

No funding was received for this study.

Acknowledgements

A never ending gratitude to all professionals and patients who made this and future works possible.

Supplementary data

Supplementary data related to this article can be found at https://doi.org/10.1016/j.cortex.2017.08.021.

REFERENCES

Blackford, T., Holcomb, P. J., Grainger, J., & Kuperberg, G. R. (2012 Apr 30). A funny thing happened on the way to articulation: N400 attenuation despite behavioral interference in picture naming. *Cognition, 123*(1), 84–99.

Chao, L. L., Haxby, J. V., & Martin, A. (1999 Oct 1). Attribute-based neural substrates in temporal cortex for perceiving and knowing about objects. *Nature Neuroscience, 2*(10), 913–919.

Cho-Hisamoto, Y., Kojima, K., Brown, E. C., Matsuzaki, N., & Asano, E. (2015 Jan 31). Gamma activity modulated by naming of ambiguous and unambiguous images: Intracranial recording. *Clinical Neurophysiology, 126*(1), 17–26.

Corina, D. P., Loudermilk, B. C., Detwiler, L., Martin, R. F., Brinkley, J. F., & Ojemann, G. (2010 Nov 30). Analysis of naming errors during cortical stimulation mapping: Implications for models of language representation. *Brain and Language, 115*(2), 101–112.

Cortes, C., & Vapnik, V. (1995 Sep 1). Support-vector networks. *Machine Learning, 20*(3), 273–297.

Costa, A., Strijkers, K., Martin, C., & Thierry, G. (2009 Dec 15). The time course of word retrieval revealed by event-related brain potentials during overt speech. *Proceedings of the National Academy of Sciences, 106*(50), 21442–21446.

DeLeon, J., Gottesman, R. F., Kleinman, J. T., Newhart, M., Davis, C., Heidler-Gary, J., et al. (2007 May 1). Neural regions essential for distinct cognitive processes underlying picture naming. *Brain, 130*(5), 1408–1422.

Dell, G. S. (1990 Oct 1). Effects of frequency and vocabulary type on phonological speech errors. *Language and Cognitive Processes, 5*(4), 313–349.

Dong, Y. S., & Han, K. S. (2004 Sep 15). A comparison of several ensemble methods for text categorization. In *2004 IEEE international conference on services computing, 2004. (SCC 2004). Proceedings* (pp. 419–422). IEEE.

Edwards, E., Nagarajan, S. S., Dalal, S. S., Canolty, R. T., Kirsch, H. E., Barbaro, N. M., et al. (2010 Mar 31). Spatiotemporal imaging of cortical activation during verb generation and picture naming. *NeuroImage, 50*(1), 291–301.

Efron, B. (1992). Bootstrap methods: Another look at the jackknife. In *Breakthroughs in statistics* (pp. 569–593). New York: Springer.

Eickhoff, S. B., Stephan, K. E., Mohlberg, H., Grefkes, C., Fink, G. R., Amunts, K., et al. (2005 May 1). A new SPM toolbox for

combining probabilistic cytoarchitectonic maps and functional imaging data. *NeuroImage, 25*(4), 1325–1335.
Fischl, B. (2012 Aug 15). FreeSurfer. *NeuroImage, 62*(2), 774–781.
Fromkin, V. A. (1971 Mar 1). The non-anomalous nature of anomalous utterances. *Language*, 27–52.
Garrett, M. F. (1980). Levels of processing in sentence production. *Language Production, 1*, 177–220.
Graves, W. W., Grabowski, T. J., Mehta, S., & Gordon, J. K. (2007 Apr). A neural signature of phonological access: Distinguishing the effects of word frequency from familiarity and length in overt picture naming. *Journal of Cognitive Neuroscience, 19*(4), 617–631.
Hamamé, C. M., Alario, F. X., Llorens, A., Liégeois-Chauvel, C., & Trébuchon-Da Fonseca, A. (2014 Aug 31). High frequency gamma activity in the left hippocampus predicts visual object naming performance. *Brain and Language, 135*, 104–114.
Hickok, G., & Poeppel, D. (2007 May 1). The cortical organization of speech processing. *Nature Reviews Neuroscience, 8*(5), 393–402.
Indefrey, P., & Levelt, W. J. (2004 Jun 30). The spatial and temporal signatures of word production components. *Cognition, 92*(1), 101–144.
Laganaro, M., & Perret, C. (2011 Mar 1). Comparing electrophysiological correlates of word production in immediate and delayed naming through the analysis of word age of acquisition effects. *Brain Topography, 24*(1), 19–29.
Llorens, A., Trébuchon, A., Liégeois-Chauvel, C., & Alario, F. X. (2011). Intra-cranial recordings of brain activity during language production. *Frontiers in Psychology*, 2.
Martin, S., Millán, J. D., Knight, R. T., & Pasley, B. N. (2016 Jul 1). The use of intracranial recordings to decode human language: Challenges and opportunities. *Brain and Language*. http://dx.doi.org/10.1016/j.bandl.2016.06.003. pii: S0093-934X(15)30124-3.
Munding, D., Dubarry, A. S., & Alario, F. X. (2016 Apr 20). On the cortical dynamics of word production: A review of the MEG evidence. *Language, Cognition and Neuroscience, 31*(4), 441–462.
Pedregosa, F., Varoquaux, G., Gramfort, A., Michel, V., Thirion, B., Grisel, O., et al. (2011 Oct). Scikit-learn: Machine learning in Python. *Journal of Machine Learning Research, 12*, 2825–2830.
Pieper, S., Halle, M., & Kikinis, R. (2004 Apr 15). 3D slicer. In *2004 IEEE international symposium on biomedical imaging: Nano to macro* (pp. 632–635). IEEE.
Salti, M., Monto, S., Charles, L., King, J. R., Parkkonen, L., & Dehaene, S. (2015 May 21). Distinct cortical codes and temporal dynamics for conscious and unconscious percepts. *Elife, 4*, e05652.
Schölkopf, B., & Smola, A. J. (2002). *Learning with kernels: Support vector machines, regularization, optimization, and beyond*. MIT Press.
Slagter, H. A., Mazaheri, A., Reteig, L. C., Smolders, R., Figee, M., Mantione, M., et al. (2017 Feb 1). Contributions of the ventral striatum to conscious perception: An intracranial EEG study of the attentional blink. *Journal of Neuroscience, 37*(5), 1081–1089.
Snodgrass, J. G., & Vanderwart, M. (1980 Mar). A standardized set of 260 pictures: norms for name agreement, image agreement, familiarity, and visual complexity. *Journal of Experimental Psychology: Human Learning and Memory, 6*(2), 174.
Strijkers, K., & Costa, A. (2016 Apr 20). The cortical dynamics of speaking: Present shortcomings and future avenues. *Language, Cognition and Neuroscience, 31*(4), 484–503.
Tanji, K., Suzuki, K., Delorme, A., Shamoto, H., & Nakasato, N. (2005 Mar 30). High-frequency $\tilde{I}^3$-band activity in the basal temporal cortex during picture-naming and lexical-decision tasks. *The Journal of Neuroscience, 25*(13), 3287–3293.
Welch, P. D. (1967 Jun). The use of fast Fourier transform for the estimation of power spectra: A method based on time averaging over short, modified periodograms. *IEEE Transactions on Audio and Electroacoustics, 15*(2), 70–73.
Wilson, S. M., Isenberg, A. L., & Hickok, G. (2009 Nov 1). Neural correlates of word production stages delineated by parametric modulation of psycholinguistic variables. *Human Brain Mapping, 30*(11), 3596–3608.